Dynamics and stability of an optically levitated mirror

Ruvi Lecamwasam,[1],[*] Alistair Graham,[1] Jinyong Ma,[1] Kabilan Sripathy,[1] Giovanni Guccione,[1] Jiayi Qin,[1] Geoff Campbell,[1] Ben Buchler,[1] Joseph J. Hope [ORCID],[2] and Ping Koy Lam [ORCID][1]

[1]*Centre for Quantum Computation and Communication Technology, Department of Quantum Science, Research School of Physics, Australian National University, Canberra, Australian Capital Territory 2601 Australia*
[2]*Department of Quantum Science, Research School of Physics, Australian National University, Canberra, Australian Capital Territory 2601 Australia*

We analyze the dynamics of a one-dimensional vertical Fabry-Pérot cavity, where the upper mirror levitates due to intracavity radiation pressure force. A perturbative approach is used based around separation of timescales, which allows us to calculate the physical quantities of interest. Due to the dynamics of the cavity field, we find that the upper mirror's motion will always be unstable for levitation performed using only a single laser. Stability can be achieved for two lasers, where one provides the trapping potential and the other a damping effect, and we locate and characterize all parameter regimes where this can occur. Finally we analyze photothermal effects due to heating of the mirror substrate. We show that this can stabilize the system, even with only a single input laser, if it acts to increase the optical path length of the cavity. This work serves as a foundation for understanding how levitated optical cavity schemes can be used as stable metrological platforms.

I. INTRODUCTION

Optomechanics explores the interaction between electromagnetic radiation and mechanical motion. The canonical example is a Fabry-Pérot cavity, one end of which oscillates on a spring [1]. This interaction between different physical systems opens up many applications. We can perform precision metrology by coupling the mechanical motion to some force of interest and reading out its position via the cavity field [2], and thermal motion of the oscillator can be cooled using optical techniques [3]. A quantum state of light in the cavity could generate a macroscopic quantum superposition in the mechanical oscillator [4,5], providing a platform for tests of quantum decoherence [6] and models of semiclassical quantum gravity [7–9]. Alternatively, the interaction can lead to the generation of squeezed light for quantum information [10,11].

The main source of noise and decoherence in optomechanical systems is generally thermal effects from the environment, which will couple into the system via the mechanical oscillator and can be significant even at cryogenic temperatures [12]. Finding ways to combat this is one of the key challenges in optomechanics. One approach is to use advanced fabrication techniques and designs to reduce the coupling via the physical channel [13,14]. Alternatively, we can replace the mechanical spring with optical trapping and levitation of the cavity mirrors [15–21], which can also lead to optical springs with much higher Q factors than is possible mechanically [22,23] due to the lack of internal mechanical strains in the oscillation. In particular, we will consider a vertically oriented Fabry-Pérot cavity where the upper mirror levitates on the intracavity field. This approach achieves decoupling from the environment, without the drawback of scattering losses present in setups

such as optical tweezers. These systems are also open to further, all-optical system engineering [24].

Such a system has been proposed and analyzed [8,25–27], and it has been found that these can attain the standard quantum limit with realistic experimental parameters. These schemes are also very flexible, with the spring constant and damping coefficient selectable through choice of optical frequency and power [20]. However, a detailed investigation of the optical spring has not yet been performed. While the levitating mirror shares many characteristics with conventional optomechanical systems, the lack of a reference mechanical oscillator means that the spring is entirely optical in nature. We will show that this introduces some key differences in behavior.

In this paper we perform a theoretical investigation of the optical spring of a one-dimensional levitating system, making use of a perturbative and separation-of-timescales approach. While our analysis will be fully classical, such a treatment is a necessary precursor to both a quantum investigation and experimental realization. We will be concerned only with optically induced stability, with the assumption that geometric stability has already been provided. This could be done via a field gradient as in optical tweezers [28,29], a multibeam configuration [25,26], or other means such as electromagnetic confinement.

In Sec. II we introduce a perturbative analysis based on separation of the optical and mechanical timescales. Key dimensionless parameters are identified in Sec. II A, and an adiabatic approximation in Sec. II B allows us to identify an effective potential in which the levitating mirror moves. In Sec. II C we consider the first-order correction to this which introduces optical antidamping to the system, and in Sec. II D we show how the previous analysis leads to an intuitive visualization of the evolution of our dynamical variables. We then apply this formalism in Sec. III, analyzing passive two-laser

---
[*]ruvi.lecamwasam@anu.edu.au

TABLE I. Physical parameters used in the model.

Variable	Meaning
	Mirror
x	Mirror height
p_x	Mirror momentum
m	Mirror mass
g	Gravitational acceleration
	Cavity
L_0	Cavity natural length
G	Linear optomechanical coupling ω_0/L
ω_0	Cavity frequency
κ_i	Cavity input coupling
$\delta\omega$	Cavity linewidth
	First input laser
α	Amplitude of first cavity field
P_α	Input power of first input laser
ω_α	Frequency of first input laser
Δ_α	First laser detuning $\omega_0 - \omega_\alpha$
	Second input laser
β	Amplitude of second cavity field
P_β	Input power of second input laser
ω_β	Frequency of second input laser
Δ_β	Second laser detuning $\omega_0 - \omega_\beta$
	Photothermal effects
ζ	Photothermal strength
γ	Photothermal relaxation rate

TABLE II. Natural parameters used in the model.

Variable	Meaning
	Natural scales
ℓ	Natural length $\frac{\delta\omega/2}{G}$
ν	Mechanical frequency $\sqrt{G^2 P_\alpha 2\kappa_i/m\omega_0(\delta\omega/2)^3}$
	Cavity and Mirror
$\tilde{x}$	x/ℓ
$\tilde{p}_x$	$p_x/m\ell\nu$
$\tilde{\sigma}$	$\sqrt{\tilde{g}^{-1} - 1}$
$\tilde{g}$	Effective gravity $(mgL_0(\delta\omega/2)^2)/(2\kappa_i P_\alpha)$
$\tilde{\varepsilon}$	Ratio of timescales $\nu/(\delta\omega/2)$
$\tilde{\chi}$	$\tilde{x} + \tilde{\Delta}_\alpha$
	First input laser
$\tilde{\alpha}$	α/A
A	Cavity max amplitude $(\delta\omega/2)^{-1}\sqrt{(2\kappa_i P_\alpha)/(\hbar\omega_0)}$
$\tilde{\Delta}_\alpha$	$\Delta_\alpha/(\delta\omega/2)$
	Second input laser
$\tilde{\beta}$	$\beta/(\tilde{B}A)$
$\tilde{B}$	Ratio of max amplitudes of β/α: $\sqrt{P_\beta/P_\alpha}$
$\tilde{\Delta}_\beta$	$\Delta_\beta/(\delta\omega/2)$
$\tilde{\Delta}_{\beta\alpha}$	$\tilde{\Delta}_\beta - \tilde{\Delta}_\alpha$
	Photothermal effects
$\tilde{\zeta}$	$(\hbar\omega_0 A^2 \zeta)/(2\ell L_0/c)l$
$\tilde{\gamma}$	γ/ν

optical cooling in Sec. III A and photothermal expansion in Sec. III B.

The quantities defined in the paper are summarized in Tables I and II. Code for computer simulations, their results, and all figures may be downloaded from Ref. [30].

II. ANALYSIS OF THE IDEAL SYSTEM

We first consider an idealized version of our system. This can be very well characterized, and our findings and intuition can be translated to when we add in experimental considerations such as additional lasers and photothermal expansion.

The system is shown in Fig. 1, and consists of a vertically oriented Fabry-Pérot cavity where the bottom mirror is fixed and the upper levitates due to the radiation pressure force of the intracavity field. The cavity has frequency ω_0 and natural length L_0, and the deviation of the upper mirror's position from L_0 is denoted by x. The intracavity field amplitude is α. In what follows, we will often refer to the levitating mirror as simply the "mirror."

We will often want to compute the values of various quantities. A typical set of parameters for this system is a cavity finesse of 2500, a length of 10 cm, and a mirror mass of 1 mg. We will take the input laser to be 1050 nm with a power of 2 watts, and assume the input coupling is half of the linewidth ($\kappa_i = \delta\omega/2$ in Eq. (1)), meaning all losses are coming from the bottom mirror.

A. Dimensionless equations of motion

Suppose the cavity is driven by a coherent laser field with frequency ω_α. Moving to a reference frame rotating with the laser frequency, the system is then described by the equations

of motion [1, Sec. III.C] (where a dot denotes a derivative with respect to time t)

$$\dot{x} = \frac{p_x}{m},$$
$$\dot{p}_x = -mg + \hbar G|\alpha|^2, \qquad (1)$$
$$\dot{\alpha} = i(\Delta_\alpha + Gx)\alpha - \frac{\delta\omega}{2}\alpha + \sqrt{\frac{2\kappa_i P_\alpha}{\hbar\omega_0}}.$$
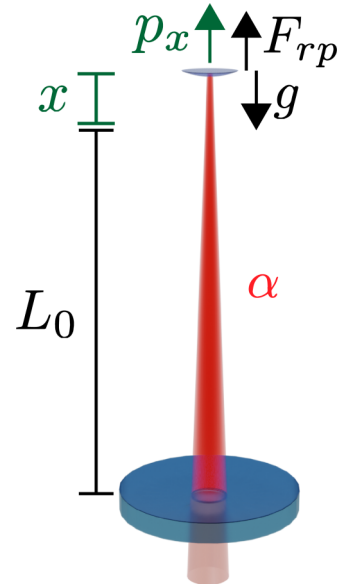

FIG. 1. A vertically oriented Fabry-Pérot cavity with frequency ω_0, natural length L_0, and intracavity field amplitude α. The upper mirror is displaced a distance x and has momentum p_x. The mirror is pushed downwards by gravity g, and upwards by radiation pressure force $F_{\rm rp} = \hbar G|\alpha|^2$.

Here m is the mass of the mirror, with x and p_x its position and momentum, respectively, and g the gravitational acceleration. In the second equation the $\hbar G|\alpha|^2$ term represents the radiation pressure force on the mirror due to the cavity field, with G the linearized optomechanical coupling [1, Sec. III.B]. The input field of power P_α is detuned $\Delta_\alpha = \omega_0 - \omega_\alpha$ relative to the cavity resonance, with input coupling κ_i. The cavity has linewidth $\delta\omega$, and $\hbar$ is the reduced Planck's constant.

To simplify the analysis, we nondimensionalize the equations of motion. What follows is a brief discussion of the results, for more details see Appendix A. We will introduce a natural length scale ℓ, frequency ν, and cavity amplitude A, defined as

$$\ell = \frac{\delta\omega/2}{G}, \quad \nu = \sqrt{\frac{\hbar G A^2}{m\ell}}, \quad A = \frac{1}{\delta\omega/2}\sqrt{\frac{2\kappa_i P_\alpha}{\hbar\omega_0}}. \quad (2)$$

The parameter ℓ is the spatial displacement of the mirror for the cavity to have a detuning of one half-linewidth, and A gives the maximum cavity amplitude: $0 < |\alpha|^2 < |A|^2$. The timescale of the upper mirror's oscillation frequencies is given by ν, which is half the optical spring frequency at one lindwidth's displacement. Because of this we will often refer to ν as the "mechanical timescale" and $\delta\omega/2$ as the "optical timescale."

In terms of these natural scales we define the dimensionless dynamical variables (denoted by a tilde):

$$\tilde{\tau} = \nu t, \quad \tilde{x} = \frac{x}{\ell}, \quad \tilde{p} = \frac{p}{m\ell\nu}, \quad \tilde{\alpha} = \frac{\alpha}{A}. \quad (3)$$

Because of the chosen normalization, we will have $0 < |\tilde{\alpha}|^2 < 1$. Furthermore the mirror variables $\tilde{x}$ and $\tilde{p}_x$ will typically be of order 1, as if $\tilde{x} \gg 1$ the cavity detuning will be far from resonance so the optical force will approach zero.

We will also require three dimensionless parameters:

$$\tilde{g} = \frac{g}{\ell\nu^2}, \quad \tilde{\varepsilon} = \frac{\nu}{\delta\omega/2}, \quad \tilde{\Delta}_\alpha = \frac{\Delta_\alpha}{\delta\omega/2}. \quad (4)$$

The simplest is $\tilde{\Delta}_\alpha$, which is the detuning rescaled in terms of the cavity linewidth. More interesting is the "effective gravity" $\tilde{g}$, which equals (simplifying $G = \omega_0/L_0$ [1, Sec. III.B])

$$\tilde{g} = \frac{mgL_0(\delta\omega/2)^2}{2\kappa_i P_\alpha}. \quad (5)$$

In the numerator are quantities which, when increased, make levitation more difficult, namely mass, gravity, cavity linewidth, and the natural length of the cavity. In the denominator we have the coupled input power.

Finally there is the parameter $\tilde{\varepsilon}$, which compares the response timescale of the cavity $\delta\omega/2$ to our natural timescale ν:

$$\tilde{\varepsilon} = \frac{1}{L_0(\delta\omega/2)^{5/2}}\sqrt{\frac{2\kappa_i P_\alpha \omega_0}{m}}. \quad (6)$$

To understand the dependence on cavity length it is helpful to expand $\delta\omega = (\pi c)/(L_0\mathcal{F})$, where c is the speed of light and $\mathcal{F}$ the cavity finesse

$$\tilde{\varepsilon} = L_0^{3/2}\left(\frac{2\mathcal{F}}{\pi c}\right)^{5/2}\sqrt{\frac{2\kappa_i P_\alpha \omega_0}{m}}. \quad (7)$$

Typically the intracavity field responds very quickly to changes in the position of the mirror, and so $\tilde{\varepsilon}$ will be very small. For the parameters mentioned in Sec. II B we have $\tilde{\varepsilon} \approx 1/6$, and if the cavity length is decreased to 1 cm this becomes $\tilde{\varepsilon} \approx 1/60$. We will exploit this separation of timescales to perform a perturbative expansion around $\tilde{\varepsilon} \approx 0$, which will simplify the dynamics to the point where an analytic approach is tractable. Numerical simulation will show that this picture is still reasonably accurate, even for values of $\tilde{\varepsilon} \approx 1/5$.

With these definitions, and letting primes denote derivatives with respect to $\tilde{\tau}$, the equations of motion are

$$\begin{aligned} \tilde{x}' &= \tilde{p}_x, \\ \tilde{p}_x' &= -\tilde{g} + |\tilde{\alpha}|^2, \\ \tilde{\alpha}' &= [i(\tilde{\Delta}_\alpha + \tilde{x})\tilde{\alpha} - \tilde{\alpha} + 1]/\tilde{\varepsilon}. \end{aligned} \quad (8)$$

From the differential equation for $\tilde{p}_x'$, we see that levitation can only occur in the regime $0 < \tilde{g} < 1$. Throughout the rest of this section we will understand this system by analyzing it using successively weaker approximations.

B. Adiabatic limit

The optical timescale will typically be much faster than the mechanical one. We can exploit this to perform an "adiabatic approximation" and assume that for any given $\tilde{x}$, the light field will immediately reach its steady state given by $\tilde{\alpha}' = 0$. Formally this corresponds to the limit $\tilde{\varepsilon} \to 0$, see Appendix B for a detailed derivation. In this case we have

$$|\tilde{\alpha}|^2 = \frac{1}{1 + (\tilde{\Delta}_\alpha + \tilde{x})^2}, \quad (9)$$

giving us the reduced equations of motion

$$\begin{aligned} \tilde{x}' &= \tilde{p}_x, \\ \tilde{p}_x' &= -\tilde{g} + \frac{1}{1 + (\tilde{\Delta}_\alpha + \tilde{x})^2}. \end{aligned} \quad (10)$$

In Appendix C we show that these equations describe a classical particle moving in a potential

$$\tilde{V}(\tilde{x}) = \tilde{g}(\tilde{\Delta}_\alpha + \tilde{x}) - \arctan(\tilde{\Delta}_\alpha + \tilde{x}), \quad (11)$$

with total dimensionless energy

$$\tilde{\mathcal{E}}(\tilde{x}, \tilde{p}_x) = \frac{\tilde{p}_x^2}{2} + \tilde{V}(\tilde{x}). \quad (12)$$

We plot the potential $\tilde{V}(\tilde{x})$ in Fig. 2(a) for various values of $\tilde{g}$. This has two equilibrium points at

$$\tilde{x}_\pm^s = -\tilde{\Delta}_\alpha \pm \tilde{\sigma}, \quad (13)$$

where we defined

$$\tilde{\sigma} = \sqrt{\tilde{g}^{-1} - 1}. \quad (14)$$

The point $\tilde{x}_-^s$ is unstable, while $\tilde{x}_+^s$ allows for quasistable oscillations. Small $\tilde{g}$ gives a wide and shallow potential well, which morphs into a point of inflection as $\tilde{g}$ approaches its maximum value of 1.

We detail in Appendix C how to use $\tilde{V}(\tilde{x})$ to calculate the possible frequencies of oscillation of the mirror, which will depend on the amplitude of oscillation since the well
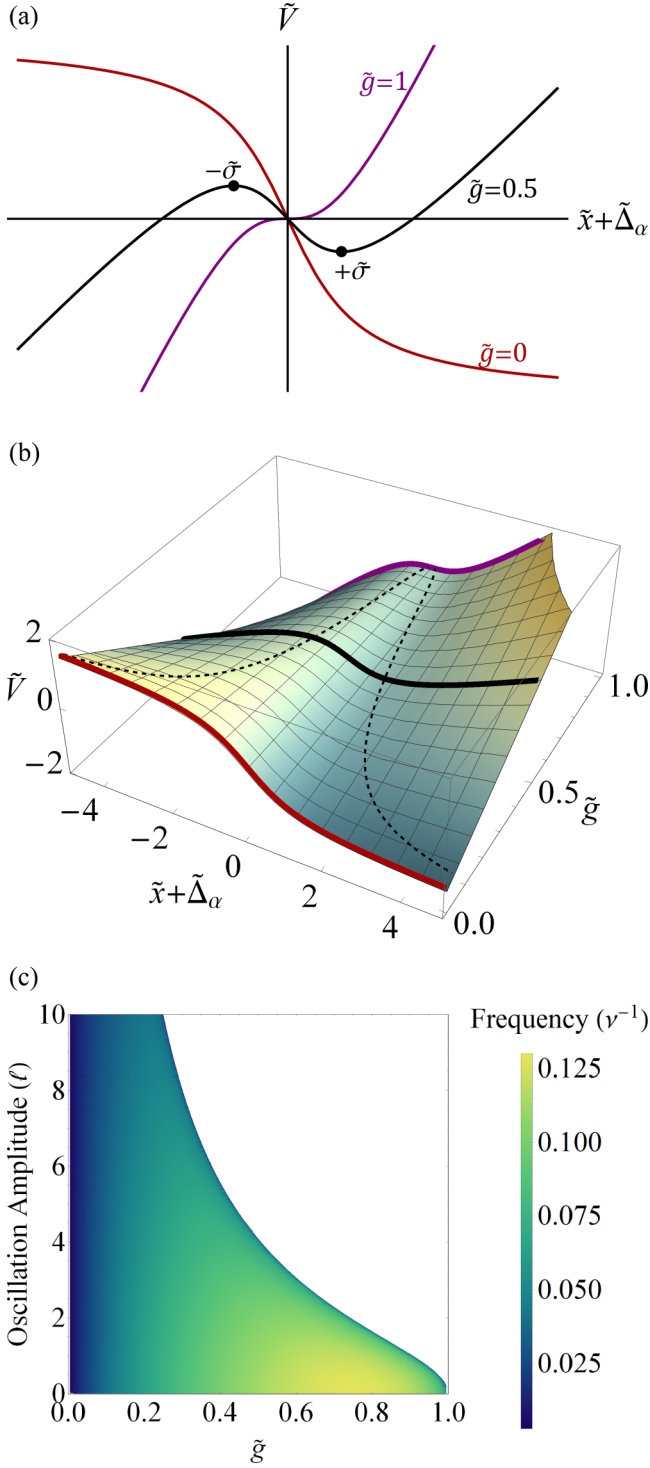
FIG. 2. (a) Slices of the dimensionless potential Eq. (11), plotted for various values of $\tilde{g}$. The two black dots represent the equilibrium points at $\pm\tilde{\sigma}$ for $\tilde{g} = 0.5$. (b) The dimensionless potential over all values of $\tilde{g}$. The solid lines correspond to the values of $\tilde{g}$ plotted in (a), and the dashed lines show the equilibria at $\pm\tilde{\sigma}$. (c) The frequencies of oscillation divided by $\tilde{\nu}$, as a function of $\tilde{g}$ and amplitude scaled by ℓ. The white region represents oscillation amplitudes which are larger than the width of the potential well for that value of $\tilde{g}$, and hence impossible.

is anharmonic. The range of possible amplitudes decreases as $\tilde{g}$ increases, as this corresponds to the well shortening. We plot the frequencies in Fig. 2(c). Note that apart from amplitude, the frequency of oscillation depends solely on the dimensionless parameter $\tilde{g}$, and we observe that frequency decreases as the amplitude increases.

Finally, up to present we assumed that the detuning $\tilde{\Delta}_\alpha$ is static. In practice the system is often characterized by sweeping the detuning over a range of values: $\tilde{\Delta}_\alpha(\tilde{\tau}) = \tilde{\Delta}_{\alpha 0} + \tilde{s}\tilde{\tau}$, for $\tilde{\Delta}_{\alpha 0}$, $\tilde{s}$ constants. Assuming the mirror begins resting on some solid support at $\tilde{x} = 0$, we show in Appendix C that if the detuning is swept from negative to positive the mirror exhibits temporary oscillations, while if the detuning begins positive and decreases, the mirror will be lifted off the support if and only if the scan speed $\tilde{s}$ is less than the critical value

$$\tilde{s}_c = 2\sqrt{\arctan(\tilde{\sigma}) - \tilde{\sigma}\tilde{g}}. \tag{15}$$

C. Dynamics of the light field

We will now relax the adiabatic approximation, and consider the first-order perturbation to Eq. (10) induced by the dynamics of the light field. In Appendix B we derive the first-order correction

$$\tilde{x}' = \tilde{p}_x,$$

$$\tilde{p}'_x = -\tilde{g} + \frac{1}{1 + (\tilde{x} + \tilde{\Delta}_\alpha)^2} + \tilde{\varepsilon}\frac{4(\tilde{p}_x + \tilde{s})(\tilde{x} + \tilde{\Delta}_\alpha)}{[1 + (\tilde{x} + \tilde{\Delta}_\alpha)^2]^3}. \tag{16}$$

Recall that in the adiabatic limit the mirror oscillated in the dimensionless potential without any loss of energy. If we compute the derivative of $\tilde{\mathcal{E}}$, hereafter referred to as the "heating rate," from Eq. (12) with respect to the first-order equations Eq. (16), we find (setting $\tilde{s} = 0$ for simplicity)

$$\frac{d\tilde{\mathcal{E}}}{d\tilde{\tau}} = \tilde{\varepsilon}\frac{4\tilde{p}_{\tilde{x}}^2(\tilde{x} + \tilde{\Delta}_\alpha)}{[1 + (\tilde{x} + \tilde{\Delta}_\alpha)^2]^3}. \tag{17}$$

The dynamics of the light field thus alters the energy of the system, and the sign of $\tilde{x} + \tilde{\Delta}_\alpha$ determines whether damping (negative) or antidamping (positive) occurs. This corresponds to the usual optomechanical picture of sideband-heating (cooling) in the blue (red-detuned) input-laser regime [1, Sec. VA]. Let us look again at the potential in Fig. 2(a), and consider a small oscillation around the potential well minimum. Since the oscillations lie to the right of the axis, $\tilde{x} + \tilde{\Delta}_\alpha$ is positive; there will be antidamping and the amplitude of the oscillation will grow. Eventually the oscillations will be so large that the mirror crosses the axis into the damping region, however, as this is much narrower than the antidamping region, we can expect that over one oscillation the antidamping will dominate, and the mirror will eventually cross over $-\tilde{\sigma}$ and leave the trap. The effect of the dynamics of the light field is thus to render unstable all oscillations within the trapping well.

Finally, we investigate in Fig. 3 how accurate the approximation made in this section is. We see in Fig. 3(a) that for a value of $\tilde{\varepsilon} = 1/100$ there is no visible difference between the approximation and full simulation for $\tilde{x}$ and $\tilde{p}_x$. Zooming in on the heating rate in Fig. 3(b), this is found to be highly
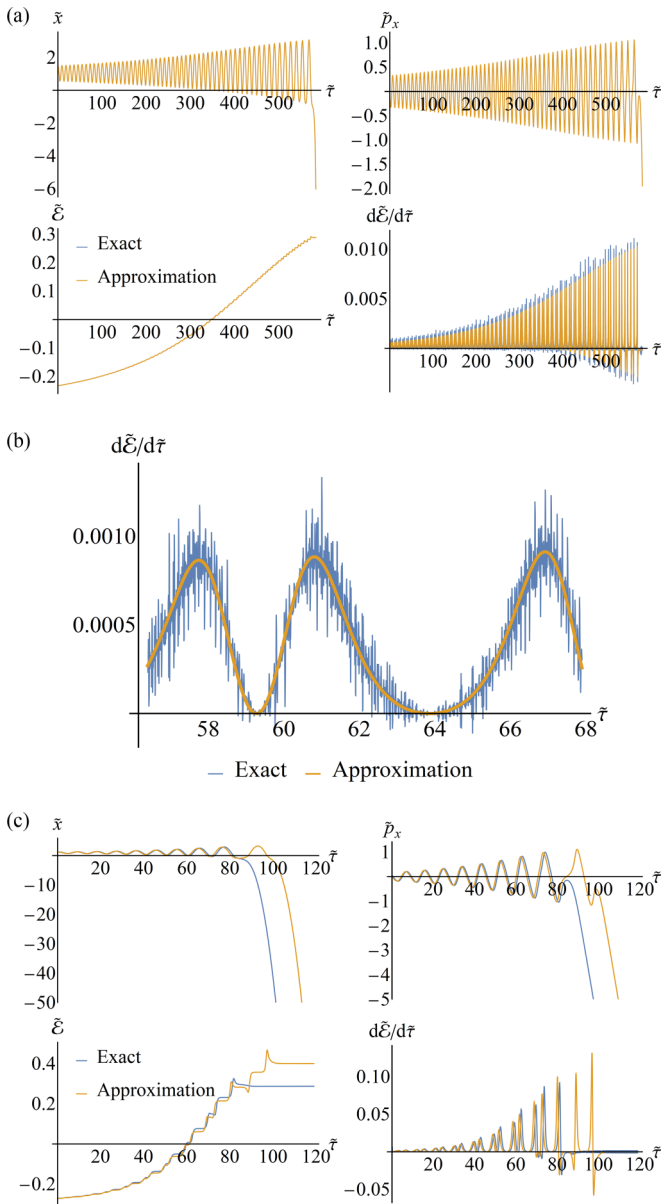
FIG. 4. (a) A plot of $\tilde{x}$ vs $\tilde{t}$ for $(\tilde{g}, \tilde{\Delta}_\alpha, \tilde{\varepsilon}) = (0.5, 0, 1/5)$, where the trajectory is colored according to time $\tilde{\tau}$ (beginning at blue and ending at yellow), and shown moving in the effective potential $\tilde{V}(\tilde{x})$ defined in Eq. (11). The mirror exhibits growing oscillations in the trapping region, until eventually it falls out. (b) The same trajectory now plotted in phase space. The dynamics rapidly collapse onto the Lorentzian-shaped adiabatic manifold given by Eq. (9), then exhibit growing oscillations until they fall out of the trap.

FIG. 3. (a) Comparison of the first-order approximation Eq. (16) (orange) with the full system Eq. (8) (blue), with parameters $(\tilde{g}, \tilde{\varepsilon}, \tilde{\Delta}_\alpha) = (0.5, 1/100, 0)$. The mirror starts off slightly perturbed from equilibrium, and exhibits growing oscillations until it falls out of the trapping well. The traces for $\tilde{x}$, $\tilde{p}_x$, and the energy $\tilde{\mathcal{E}}$ perfectly coincide, while we can see slight discrepancies in the heating rate $d\tilde{\mathcal{E}}/d\tilde{\tau}$. (b) Zooming in to the heating rate $d\tilde{\mathcal{E}}/d\tilde{t}$ (same parameters as (a)) we see that the actual equations of motion predict very fast behavior, the average of which is well described by the approximation. (c) For $\tilde{\varepsilon} = 1/10$ the actual dynamics eventually diverge from those of the approximation, however, they are still qualitatively similar.

D. Visualizing the motion

The simpler picture of the adiabatic and first-order approximations provides us with an intuitive visualization of the system dynamics. Consider the trace for position $\tilde{x}$ in Fig. 3(a); the mirror exhibits growing oscillations until at some point it falls out of the trap. We can better understand this by plotting the mirror's motion in the potential $\tilde{V}(\tilde{x})$ in Fig. 4(a) (simulated for a different value of $\tilde{\varepsilon}$ to Fig. 3). Now we can clearly see how the mirror is oscillating in a trapping region, and that the fall occurs once the oscillations take it out of the potential well. Note that we are simulating the full dynamics Eq. (8) without any approximation.

In Fig. 4(b) we plot the same trajectory in phase space. Regardless of starting point, the dynamics rapidly collapse onto the Lorentzian-shaped adiabatic manifold given by Eq. (9), indicated by the orange surface. The system exhibits growing oscillations on the manifold, until eventually falling out of the trap. Thus while we have three dynamical variables,

oscillatory due to the rapid dynamics of the cavity field, but the average value is well described by the approximation. For $\tilde{\varepsilon} = 1/10$ shown in Fig. 3(c) we get a divergence, however, the dynamics are still qualitatively similar. The approximation may thus still be effective for analyzing qualitative features of dynamics, even in reasonably large $\tilde{\varepsilon}$ regimes.
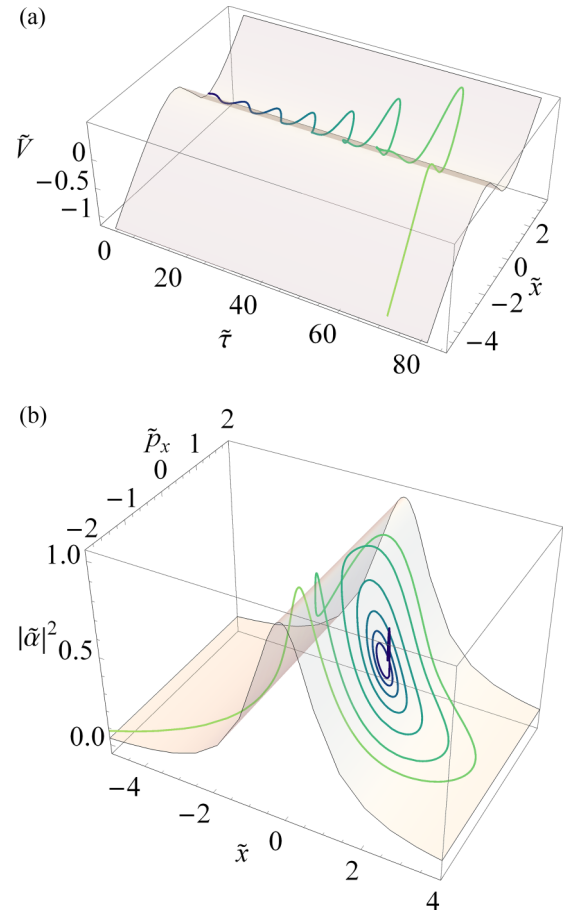
the separation of timescales means that the dynamics are effectively two-dimensional.

The potential and adiabatic manifold shown in Fig. 4 are derived in the limit $\tilde{\varepsilon} \to 0$. Note, however, that the trajectory we simulate is for the somewhat large value of $\tilde{\varepsilon} = 1/5$. Even at such values, our analysis can still provide us with an effective intuition for the system. The trajectory does briefly leave the manifold when passing over the maximum of the Lorentzian, but as $\tilde{\varepsilon}$ decreases these deviations will become much less noticeable.

III. APPLICATIONS OF IDEAL ANALYSIS

In this section we will apply the analysis of Sec. II to two scenarios of experimental relevance. First, we will look at passive sideband cooling, a commonly used technique in optomechanics, and show that it is much less effective for a levitating mirror system. Second, we investigate photothermal effects of the mirror substrate. This is likely to become significant at the powers required for levitation, and we will show that this can have a stabilising or destabilizing influence depending on the sign of the effect.

A. Passive cooling

It is common in optomechanics to use a (possibly second) laser to passively damp the mirror's motion, a technique known as sideband cooling [1, Sec. V.B]. Depending on the detuning of an input laser, it can either lead to a trapping force and antidamping, opposing motion of the mirror but transferring energy to it from the optical field, or antitrapping but damping, removing energy from the mirror while pushing it in the direction of motion. In the case of a levitated mirror the idea would be to use a strong primary laser to provide the trapping, and a weaker, detuned, ancillary laser to provide the damping. By choosing appropriate amplitudes and detunings for the two lasers, one aims to find a regime where the net trapping and damping effects dominate. In contrast to a normal optomechanical system, however, we do not have a mechanical spring, and so all of the trapping force must come from the light field. This makes a difference, and while there do exist regions with simultaneous trapping and damping, the potential around these tends to be both shallow and flat.

Suppose we have a second laser incident on the cavity, leading to another mode with amplitude β. The equations of motion Eq. (1) then become

$$
\dot{x} = \frac{p_x}{m}, \quad \dot{p}_x = -mg + \hbar G|\alpha|^2 + \hbar G|\beta|^2,
$$

$$
\dot{\alpha} = i(\Delta_\alpha + Gx)\alpha - \frac{\delta\omega}{2}\alpha + \sqrt{\frac{2\kappa_i P_\alpha}{\hbar\omega_0}},
$$

$$
\dot{\beta} = i(\Delta_\beta + Gx)\beta - \frac{\delta\omega}{2}\beta + \sqrt{\frac{2\kappa_i P_\beta}{\hbar\omega_0}},
$$

(18)

where now P_β and Δ_β are the power and detuning of the laser driving β. As before many of these parameters may be eliminated via nondimensionalization, where now we will exploit the symmetry between α, β. Without loss of generality

we may take $P_\alpha \geqslant P_\beta$, and in analogy to Eq. (3) write

$$
\tilde{\beta} = \frac{\beta}{\tilde{B}A},
$$

(19)

where $\tilde{B} = \sqrt{P_\beta/P_\alpha}$ is between zero and one, and we will also have $|\tilde{\beta}|^2 < 1$. Defining $\tilde{\Delta}_{\beta\alpha} = \tilde{\Delta}_\beta - \tilde{\Delta}_\alpha$ and $\tilde{\chi} = \tilde{x} + \tilde{\Delta}_\alpha$, the nondimensionalized equations are

$$
\tilde{\chi}' = \tilde{p}_x,
$$
$$
\tilde{p}_x' = -\tilde{g} + |\tilde{\alpha}|^2 + \tilde{B}^2|\tilde{\beta}|^2,
$$
$$
\tilde{\alpha}' = [i\tilde{\chi}\tilde{\alpha} - \tilde{\alpha} + 1]/\tilde{\varepsilon},
$$
$$
\tilde{\beta}' = [i(\tilde{\chi} + \tilde{\Delta}_{\beta\alpha})\tilde{\beta} - \tilde{\beta} + 1]/\tilde{\varepsilon}.
$$

(20)

Inspecting the equation for $\tilde{p}_x'$, for there to be levitation we must have $\tilde{g} < 1 + \tilde{B}^2$.

We first analyze this in the adiabatic approximation as in Sec. II B, leading to an effective potential which is the sum of the potentials of the individual lasers:

$$
\tilde{V}(\tilde{\chi}) = \tilde{g}\tilde{\chi} - \arctan(\tilde{\chi}) - \tilde{B}^2\arctan(\tilde{\chi} + \tilde{\Delta}_{\beta\alpha}).
$$

(21)

A first-order perturbation as in Sec. II C then gives us a heating rate

$$
\frac{d\tilde{\mathcal{E}}}{d\tilde{\tau}} = 4\tilde{p}_x^2\tilde{\varepsilon}\left(\frac{\tilde{\chi}}{(1+\tilde{\chi}^2)^3} + \tilde{B}^2\frac{(\tilde{\chi} + \tilde{\Delta}_{\beta\alpha})}{[1+(\tilde{\chi} + \tilde{\Delta}_{\beta\alpha})^2]^3}\right).
$$

(22)

These equations can be used to find regions which are both trapping (minima of $\tilde{V}(\tilde{\chi})$) and damping (negative $d\tilde{\mathcal{E}}/d\tilde{\tau}$). Equivalently we could linearize the equations of motion and search for parameter regimes where the Jacobian has negative eigenvalues. Our approach, however, also allows us to visualize the width and shape of the trapping potential and (anti)damping. There are three dimensionless parameters to search over: $0 \leqslant \tilde{B} \leqslant 1$, $0 \leqslant \tilde{g} \leqslant 1 + \tilde{B}^2$, and $\tilde{\Delta}_{\beta\alpha}$, as $\tilde{\varepsilon}$ changes only the magnitude of the (anti)damping but not its sign. While there is no bound on the detuning, we restrict ourselves to $-10 \leqslant \tilde{\Delta}_{\beta\alpha} \leqslant 10$. The code and simulation results are available for download at Ref. [30].

One trapping and damping solution is plotted in Fig. 5(a). The dashed lines denotes the "trapping region," and trajectories beginning with these will exhibit decaying oscillations towards the minimum. As we can see, a trajectory beginning in a location where the optical field is antidamping may still show net damping over one oscillation and be trapped, if, for example, it spends more time in the damping region over each period. The width of this trap is the space between the dashed lines ($\sim 1.3\,\ell$), and the depth is the vertical distance between the minimum and the intersection of the rightmost dashed line with the potential ($\sim 0.03\,m\ell^2\nu^2$) since, if the mirror moves above this, then it will leave the trapping region. The energy value the depth represents is very small, for the parameters in Sec. II this corresponds to the kinetic energy of a mirror with speed 10^{-5} ms^{-1}. However, note that from Eq. (17) the damping rate is proportional to momentum, and simulations show that an initial velocity at least ten times larger is still trapped and damped, though increasing by another factor of ten leads to the mirror escaping.

In Fig. 5(b) we take $\tilde{\varepsilon} = 1/5$ and plot the dimensionless parameters at which there exist regions of simultaneous trapping and damping. We searched over 500 values of $\tilde{g}$, 500 values
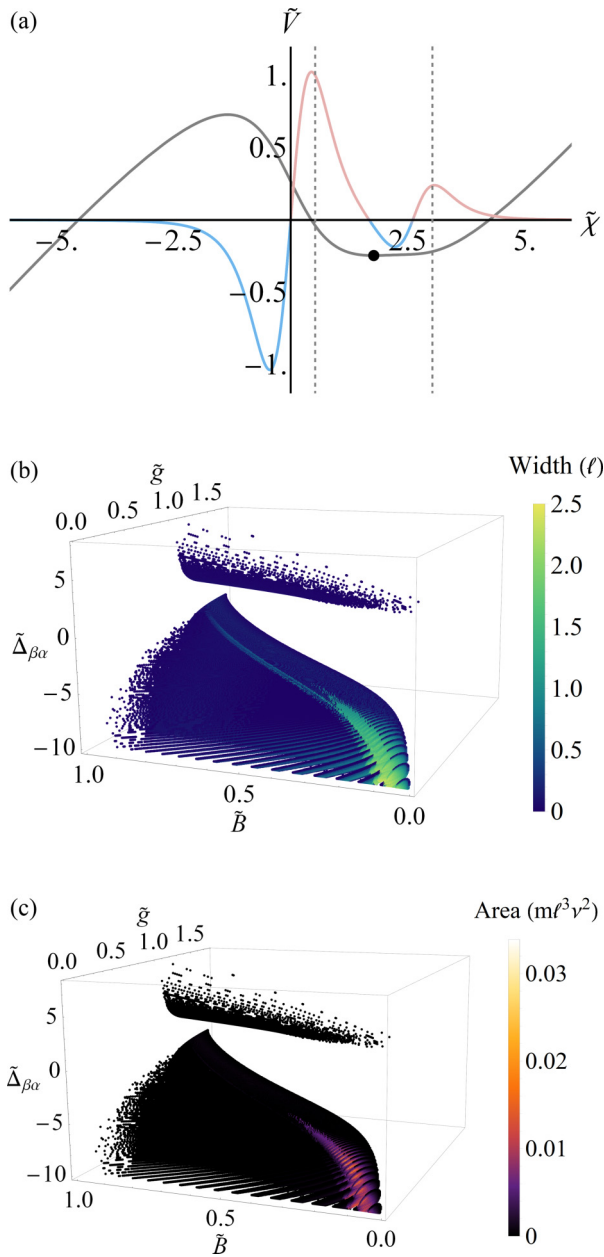
FIG. 5. (a) Regime with the greatest simultaneous trapping and damping area $(\tilde{g}, \tilde{B}, \tilde{\Delta}_{\beta\alpha}, \tilde{\varepsilon}) \approx (0.37, 0.47, -2.63, 1/5)$. The black curve shows the effective two-laser potential Eq. (21) with the black dot the minimum, and the colored line gives the effective heating rate Eq. (22) divided by $4\tilde{p}_x^2 \tilde{\varepsilon}$, with blue for damping and red antidamping. The two dashed vertical lines denote the two ends of the trapping region; trajectories originating in the trapping region with zero initial momentum will exhibit decaying oscillations towards the minimum. The distance between them is the "width" of this trap, and the vertical distance from the minimum to the intersection of the right dashed line with the potential is the "depth." Multiplying the width by the depth then gives us the "area." (b) The parameters which allow for simultaneous trapping and damping regions map out a two-dimensional folded manifold in parameter space, with $\tilde{\varepsilon} = 1/5$. Little difference is visible when $\tilde{\varepsilon} = 1/100$ (although the (anti)damping rates will be much less). The points are colored by the width of the region in units of ℓ. (c) The points are now colored by the area of the trapping and damping regions, found by multiplying the width by the depth.

of $\tilde{B}$, and 1000 values of $\tilde{\Delta}_{\beta\alpha}$ within the aforementioned ranges, in a computation which took two days on a Google Cloud Compute Engine with 64 virtual CPUs. These form a folded, two-dimensional surface, where the banding comes from the numerical grid used. The color of the points denotes the width of the trapping region. This was found by simulating the unapproximated equations of motion Eq. (20), with $\tilde{\chi}$ beginning at increasingly large distances $\tilde{\chi}_0$ from the potential well minimum, and recording the largest distance such that both a positive and negative perturbation of that magnitude to the position would remain trapped. The initial conditions for the other dynamical variables were their steady states for the given initial value of $\tilde{\chi}_0$: $\tilde{p}_x = 0$, $\tilde{\alpha} = 1/(1 - i\tilde{\chi}_0)$, and $\tilde{\beta} = 1/[1 - i(\tilde{\chi}_0 + \tilde{\Delta}_{\beta\alpha})]$. We can see that in general there are reasonably wide trapping and damping regions in the regime where both $\tilde{g}$ and $\tilde{B}$ approach zero, and $\tilde{\Delta}_{\beta\alpha}$ is strongly negatively detuned.

In Fig. 5(c) we color the points by the "area," approximately found by multiplying the width by the depth of the well. All of the trapping regions are very shallow, and so while robust against large changes in $\tilde{\chi}$, even a small change in momentum may be enough for the mirror to escape. We note that Fig. 5(a) plotted the solution with the greatest trapping area, and other solutions display similar characteristics, with a broad flat region about the minimum and a somewhat shallow nature. Thus the experimental utility of sideband cooling for levitated systems is far from guaranteed, and a detailed investigation needs to be done to study the robustness of the parameter regimes identified against fluctuations of the cavity field or the mirror's thermal Brownian motion.

Finally, we repeated the simulations for $\tilde{\varepsilon} = 1/100$ but there was little difference in the cooling widths and areas. The change in energy of the mirror's oscillations, however, either damping or antidamping, was much slower. This is to be expected, as (anti)damping arises from the dynamics of the light field, and as $\tilde{\varepsilon} \to 0$ these dynamics vanish.

B. Photothermal effects

So far we assumed the mirror to be perfectly reflecting, which will not be true in practice. The intracavity field in this system must be very strong to provide levitation, and so even for a highly reflective mirror a substantial amount of optical energy is likely to be absorbed by the mirror substrate. This induces photothermal effects, where the mirror both deforms and undergoes a change in refractive index, resulting in a measurable change to the effective optical path length of the cavity. We can model this as [31–34]

$$\dot{x} = \frac{p_x}{m}, \quad \dot{p}_x = -mg + \hbar G |\alpha|^2,$$

$$\dot{z} = -\gamma \left(z + \zeta \frac{\hbar \omega_0 |\alpha|^2}{2L_0/c} \right),$$

$$\dot{\alpha} = i[\Delta_\alpha + G(x + z)] - \frac{\delta\omega}{2}\alpha + \sqrt{\frac{2\kappa_i P_\alpha}{\hbar \omega_0}}. \tag{23}$$

The variable z represents the change in optical path length due to photon absorption by the mirror, and may be positive or negative depending on the mirror substrate. The intracavity power is given by $\frac{\hbar \omega_0 |\alpha|^2}{2L_0/c}$ (energy divided by photon travel

time), and so ζ parameterizes the rate at which intracavity power translates to a change in path length, with units' length divided by power. The timescale of the effect is quantified by the photothermal relaxation rate γ.

As in Sec. II A we may derive nondimensionalized equations of motion:

$$\tilde{x}' = \tilde{p}_x,$$
$$\tilde{p}_x' = -\tilde{g} + |\tilde{\alpha}|^2,$$
$$\tilde{z}' = -\tilde{\gamma}[\tilde{z} + \tilde{\zeta}|\tilde{\alpha}|^2],$$
$$\tilde{\alpha}' = [i(\tilde{\Delta}_\alpha + \tilde{x} + \tilde{z})\tilde{\alpha} - \tilde{\alpha} + 1]/\tilde{\varepsilon}, \quad (24)$$

where we introduced dimensionless parameters

$$\tilde{z} = \frac{z}{\ell}, \quad \tilde{\gamma} = \frac{\gamma}{\nu}, \quad \tilde{\zeta} = \frac{\hbar\omega_0 A^2 \zeta}{(2L_0/c)\ell}. \quad (25)$$

We will consider the regime $\tilde{\gamma} \ll 1$, which is true for many systems due to the slow rate of thermal expansion and contraction. For example, a typical value of γ between 10–100 Hz [35] will make $\tilde{\gamma} \sim 10^{-5} - 10^{-4}$ (for the parameters from Sec. II). The expansion coefficient ζ depends on the mirror substrate and the width and shape of the optical beam, a typical value is on the order of 10 picometers per watt [36, Sec. III.C] which corresponds to $\tilde{\zeta} \sim 30$.

We now analyze how the photothermal expansion affects the equilibrium states of the system. From $\tilde{x}'$ we clearly must have $\tilde{p}_x^s = 0$. The equation for $\tilde{p}_x'$ gives that $|\tilde{\alpha}^s|^2 = \tilde{g}$, and so from $\tilde{z}'$ we find

$$\tilde{z}^s = -\tilde{\zeta}\tilde{g}. \quad (26)$$

Thus the only contribution of the photothermal effect to the steady state is to add a constant shift to the detuning. As before the mirror position $\tilde{x}$ will have two equilibrium states

$$\tilde{x}_\pm^s = -\tilde{\Delta}_\alpha^s \pm \tilde{\sigma}, \quad (27)$$

with $\tilde{\sigma}$ from Eq. (14) and effective detuning

$$\tilde{\Delta}_\alpha^s = \tilde{\Delta}_\alpha - \tilde{\zeta}\tilde{g}. \quad (28)$$

Photothermal effects may also alter the stability of the equilibria. We discuss in Appendix D that due to the small value of $\tilde{\gamma}$, these behave as a small perturbation on our system. We may still look at the mirror as moving in the potential $\tilde{V}(\tilde{x} + \tilde{z})$, only now as well as having a damping or antidamping effect from the dynamics of the light field, we have an additional photothermal contribution. Considering a small oscillation around the potential-well minimum, the change in dimensionless energy of the system over one period is

$$2\tilde{\rho}^2(1 - \tilde{g})\tilde{g}^3\tilde{\zeta}\tilde{\gamma} + \mathcal{O}(\tilde{\gamma}^2), \quad (29)$$

where $\tilde{\rho}$ is the size of the small perturbation from equilibrium. Thus positive photothermal expansion ($\tilde{\zeta} > 0$) will provide an antidamping effect, while negative photothermal expansion ($\tilde{\zeta} < 0$) will give damping. This is similar to what is observed in conventional optomechanical systems, where engineering a photothermal effect with a negative sign to stabilize the system has also been proposed [37]. Note that Eq. (29) describes photothermal effects only, which will be in competition with the damping or antidamping induced by the light field.
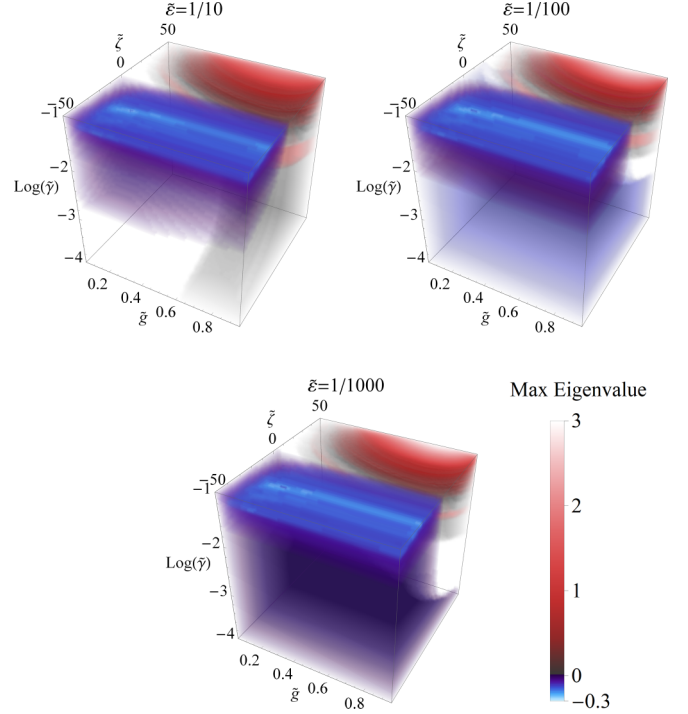

FIG. 6. We take $\tilde{\gamma} = 10^{-4}$ and compute the maximum eigenvalue of the linearized system at the potential-well minimum $\tilde{x}_+^s$ for various values of $\tilde{\varepsilon}$. Positive and negative values are colored red and blue, respectively, and the opacity is proportional to the magnitude of the eigenvalue (for negative eigenvalues a value of -0.3 is fully opaque, while for the positive eigenvalues a value of 3 is opaque). For large $\tilde{\varepsilon}$ there is competition between photothermal damping and radiation pressure antidamping, while as $\tilde{\varepsilon}$ decreases and optical effects become less significant the sign of the eigenvalues relies on $\tilde{\zeta}$ alone.

This result relied upon a number of approximations, and we can verify this with a numerical search of the unapproximated system. We compute the sign of the maximum eigenvalue around the steady state for various parameter regimes, and plot these Fig. 6. We find that $\tilde{x}_+^s$ is in general unstable for a positive $\tilde{\zeta}$, and stable for a negative value. This difference becomes more pronounced as $\tilde{\varepsilon}$ grows smaller, and the optical heating effect decreases. Interestingly, for a large positive photothermal expansion coefficient, decreasing $\tilde{\varepsilon}$ actually increases the antidamping rate.

As in Fig. 4(b), we can visualize the trajectories in phase space. Taking advantage of the almost two-dimensional nature of the dynamics we replace the $|\tilde{\alpha}|^2$-axis with the photothermal variable $\tilde{z}$, and plot this in Fig. 7(a). In this case we consider a negative photothermal expansion coefficient, and observe decaying oscillations towards the equilibrium state. These are centered on the steady state for $\tilde{x}$, $\tilde{p}_x$ assuming a fixed value $\tilde{z}$. From Eq. (27) this is given by the line

$$\tilde{x} = -\tilde{\Delta}_\alpha + \tilde{\zeta}\tilde{z} + \tilde{\sigma}, \quad (30)$$

in the $\tilde{p}_x = 0$ plane. Finally, we plot the trajectory in the dimensionless potential $\tilde{V}$ in Fig. 7(b). In this case we need to consider the total displacement $\tilde{x} + \tilde{z}$, and with this we can see
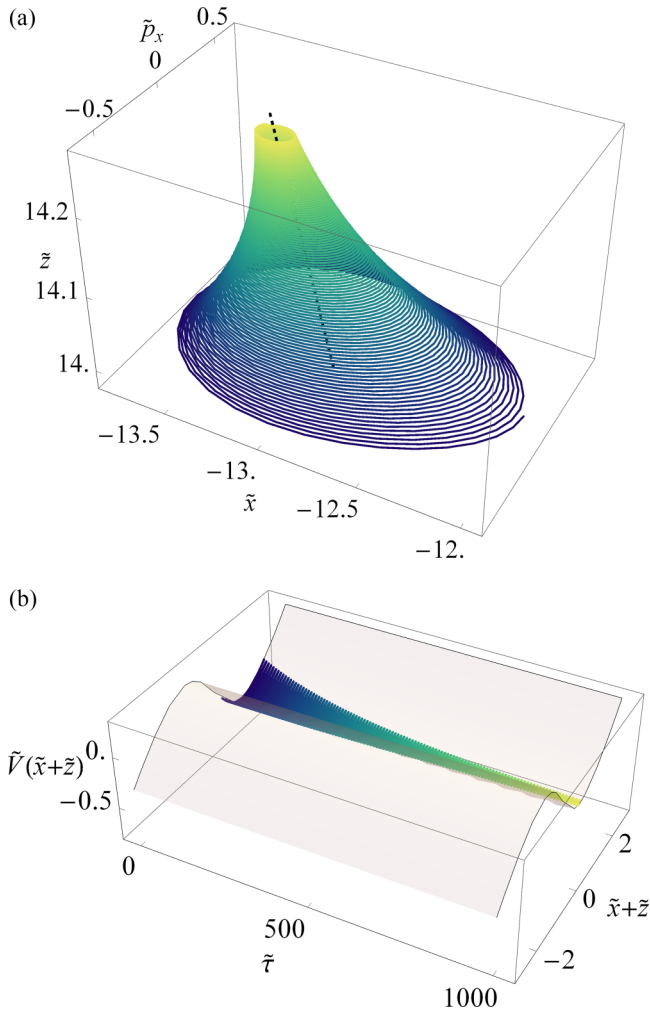
FIG. 7. (a) The phase space with photothermal expansion and a negative photothermal expansion coefficient, taking parameters $(\tilde{g}, \tilde{\Delta}_\alpha, \tilde{\varepsilon}) = (0.5, 0, 1/100)$ and $(\tilde{\zeta}, \tilde{\gamma}) = (-30, 3 \times 10^{-4})$. Time runs from blue to yellow; the trajectory begins at the bottom and exhibits decaying oscillations towards the steady state at the top. The dashed black line through the center denotes the steady state for $\tilde{x}$, $\tilde{p}_x$ assuming a fixed value of $\tilde{z}$. (b) The same trajectory, now plotted in the potential $\tilde{V}$.

the photothermal damping stabilizing the mirror oscillations towards the well minimum.

IV. CONCLUSION

We analyzed a vertically oriented Fabry-Pérot cavity where the upper mirror levitates on the intracavity radiation pressure force. Nondimensionalizing the equations of motion, the behavior was essentially determined by two dimensionless parameters: the effective gravity $\tilde{g}$ and the ratio $\tilde{\varepsilon}$ of the mechanical-to-optical timescales. Typically the optical timescale is much faster than the mechanical ($\tilde{\varepsilon} \ll 1$), and exploiting this we performed a perturbative expansion around $\tilde{\varepsilon} \approx 0$ to simplify the dynamics to the point where an analytic approach was tractable.

To zeroth order this gave an adiabatic approximation. We found an effective potential in which the upper mirror moved, and used this to calculate its frequencies of oscillation. This

also gave us an intuition for the evolution of the dynamical variables in phase space. A first-order correction to the equations of motion allowed us to derive the effective damping or antidamping rate caused by the dynamics of the cavity field. Comparing to simulations of the exact equations, our approximation was very accurate for $\tilde{\varepsilon} \sim 1/100$ and still qualitatively similar for $\tilde{\varepsilon} \sim 1/10$, which encompasses a wide range of realistic parameter regimes.

From this analysis we concluded that the motion of the upper mirror would always be unstable if the cavity was driven by a single laser, with the rate at which oscillations were amplified linearly proportional to $\tilde{\varepsilon}$. We then explored using two input lasers with different amplitudes and detunings, and found all parameter regimes which allowed for stable trapping of the upper mirror. In these regions the confining potential well could be made relatively wide, but was always flat and shallow. We also analyzed the effect of photothermal changes in the optical path length of the cavity. If heating of the mirror substrate lead to a decrease in the cavity length, working against radiation pressure force on the mirror, there was an antidamping effect. If, however, photothermal effects increased the cavity length they could stabilize the system, even with only a single laser.

Stabilizing the levitating mirror is crucial to use it as a metrological platform, and there are numerous possible ways that we could extend our analysis. One is to move beyond two lasers; it is shown in Ref. [24] that as you allow a greater number of input lasers to a conventional optomechanical system, you can approximate an arbitrarily shaped potential. It is less clear, however, if this can be done for our system while also ensuring the potential is damping, and it is likely that any multilaser potential wells which are both trapping and damping can be made very wide, but will maintain their shallow and flat nature. A promising avenue would be feedback control of the system, which should be able to stabilize it even with only a single laser. Once stabilization has been achieved, a detailed study can be performed on the various ways the levitating mirror could be used for sensing, and how to best utilize the many unique features of this platform.

APPENDIX A: DERIVATION OF ONE-DIMENSIONAL NONDIMENSIONALIZED EQUATIONS

Here we describe the nondimensionalization from Sec. II A in more detail. We will introduce a natural length scale ℓ,

frequency ν, and cavity amplitude A, defined as

$$\ell = \frac{\delta\omega/2}{G}, \quad \nu^2 = \frac{\hbar G A^2}{m\ell}, \quad A = \frac{1}{\delta\omega/2}\sqrt{\frac{2\kappa_i P_\alpha}{\hbar\omega_0}}. \quad (A1)$$

To understand these scales, we solve for the steady state of α from Eq. (1) giving the Lorentzian profile (setting $\Delta_\alpha = 0$ for simplicity)

$$|\alpha|^2 = \frac{(\delta\omega/2)^2 A^2}{(\delta\omega/2)^2 + (Gx)^2} = \frac{A^2}{1 + \left(\frac{Gx}{\delta\omega/2}\right)^2}. \quad (A2)$$

We thus see that A is the maximum intracavity amplitude. Moreover, at $x = (\delta\omega/2)/G = \ell$ the amplitude-squared has dropped to half of its maximum value, or equivalently ℓ is the distance by which the mirror moves to create a cavity detuning of one half-linewidth. In a classical optomechanical system the optical spring constant is given by the first derivative of the radiation pressure force [1, Sec. V.A]. Its value depends on x, and at $x = \ell$ we will have an optical spring constant

$$\kappa_{os}(\ell) = \frac{\partial}{\partial x}(-\hbar G|\alpha|^2)$$

$$= \frac{\hbar G^2 A^2}{\delta\omega} = 2m\frac{\hbar G A^2}{m\ell}$$

$$= m\left(\frac{\nu}{\sqrt{2}}\right)^2. \quad (A3)$$

Comparing this to the usual relation $\kappa = m\omega^2$ for a harmonic oscillator with spring constant κ, mass m, and natural frequency ω, we see that ν is $1/\sqrt{2}$ multiplied by the optical spring frequency at one half-linewidth's displacement. The "mechanical timescale" ν gives timescale of the upper mirror's oscillations, while the "optical timescale" $\delta\omega/2$ describes the speed of the cavity field's dynamics.

The dimensionless dynamical variables (denoted by a tilde) are

$$\tilde{\tau} = \nu t, \quad \tilde{x} = \frac{x}{\ell}, \quad \tilde{p} = \frac{p}{m\ell\nu}, \quad \tilde{\alpha} = \frac{\alpha}{A}. \quad (A4)$$

For the cavity field we will have $0 < |\tilde{\alpha}|^2 < 1$. Furthermore during levitation the mirror variables $\tilde{x}$ and $\tilde{p}_x$ will typically be of order 1, as if $\tilde{x} \gg 1$ the cavity detuning will be far from resonance so the optical force will approach zero.

We can now write the equations of motion in terms of the dimensionless parameters, letting a prime denote the derivative with respect to dimensionless time $\tilde{\tau}$:

$$\ell\nu\tilde{x}' = \frac{p_x}{m},$$

$$\tilde{x}' = \tilde{p}_x, \quad (A5)$$

$$m\ell\nu^2\tilde{p}_x' = -mg + \hbar G A^2|\tilde{\alpha}|^2,$$

$$\tilde{p}_x' = -\frac{g}{\ell\nu^2} + \frac{\hbar G A^2}{m\ell\nu^2}|\tilde{\alpha}|^2, \quad (A6)$$

$$= -\tilde{g} + |\tilde{\alpha}|^2,$$

$$A\nu\tilde{\alpha}' = \left(-\frac{\delta\omega}{2} + i(\Delta_\alpha + G\ell\tilde{x})\right)A\tilde{\alpha} + \sqrt{\frac{2\kappa_i P_\alpha}{\hbar\omega_0}},$$

$$\tilde{\alpha}' = \frac{\delta\omega/2}{\nu}\left[i(\tilde{\Delta}_\alpha + \tilde{x})\tilde{\alpha} - \tilde{\alpha} + \frac{1}{A(\delta\omega/2)}\sqrt{\frac{2\kappa_i P_\alpha}{\hbar\omega_0}}\right]$$

$$= [i(\tilde{\Delta}_\alpha + \tilde{x})\tilde{\alpha} - \tilde{\alpha} + 1]/\tilde{\varepsilon}. \quad (A7)$$

We defined three dimensionless parameters:

$$\tilde{g} = \frac{g}{\ell\nu^2}, \quad \tilde{\varepsilon} = \frac{\nu}{\delta\omega/2}, \quad \tilde{\Delta}_\alpha = \frac{\Delta_\alpha}{\delta\omega/2}. \quad (A8)$$

The meanings of these are explored in the main text of Sec. II A.

To summarize, the dimensionless equations of motion are

$$\tilde{x}' = \tilde{p}_x,$$

$$\tilde{p}_x' = -\tilde{g} + |\tilde{\alpha}|^2, \quad (A9)$$

$$\tilde{\alpha}' = [i(\tilde{\Delta}_\alpha + \tilde{x})\tilde{\alpha} - \tilde{\alpha} + 1]/\tilde{\varepsilon},$$

where $0 < \tilde{g}, |\tilde{\alpha}|^2 < 1$, and typically $\tilde{\varepsilon} \ll 1$. Moreover if $\tilde{\Delta}_\alpha$ is constant, we can eliminate it from our dynamics by defining $\tilde{\chi} = \tilde{\Delta}_\alpha + \tilde{x}$.

APPENDIX B: EXPANDING THE EQUATIONS OF MOTION IN ORDERS OF $\tilde{\varepsilon}$

The parameter $\tilde{\varepsilon}$ will typically be quite small, corresponding to the optical field evolving much faster than the mechanical motion of the mirror. Our dynamics Eq. (8) thus have a separation of timescales, also known in literature as a "slow-fast system." We can exploit this to simplify the dynamics in the manner of [38, Sec. 2], by expanding in a power series of $\tilde{\varepsilon}$.

We begin with

$$\tilde{\alpha} = \tilde{\alpha}_0 + \tilde{\varepsilon}\tilde{\alpha}_1 + \mathcal{O}(\tilde{\varepsilon}^2), \quad (B1)$$

and substitute this into the equation of motion for $\tilde{\alpha}'$ from Eq. (A9):

$$\tilde{\alpha}_0' + \tilde{\varepsilon}\tilde{\alpha}_1' + \mathcal{O}(\tilde{\varepsilon}^2)$$

$$= \tilde{\varepsilon}^{-1}[i(\tilde{\Delta}_\alpha + \tilde{x}) - 1][\tilde{\alpha}_0 + \tilde{\varepsilon}\tilde{\alpha}_1 + \mathcal{O}(\tilde{\varepsilon}^2)] + \tilde{\varepsilon}^{-1}. \quad (B2)$$

Equating terms of order $\tilde{\varepsilon}^{-1}$ (or equivalently multiplying both sides by $\tilde{\varepsilon}$ then taking the limit $\tilde{\varepsilon} \to 0$) gives

$$0 = [i(\tilde{\Delta}_\alpha + \tilde{x}) - 1]\tilde{\alpha}_0 + 1, \quad (B3)$$

and solving this for $\tilde{\alpha}_0$ recovers the adiabatic approximation we discussed in Sec. II B:

$$\tilde{\alpha}_0 = \frac{1}{1 - i(\tilde{\Delta}_\alpha + \tilde{x})}. \quad (B4)$$

We can thus see that the adiabatic equations of motion Eq. (10) correspond to expanding the full equations of motion Eq. (A9) to zeroth order in $\tilde{\varepsilon}$.

The terms of order 1 give

$$\tilde{\alpha}_0' = [i(\tilde{\Delta}_\alpha + \tilde{x}) - 1]\tilde{\alpha}_1, \quad (B5)$$

which has solution

$$\tilde{\alpha}_1 = \frac{-\tilde{\alpha}_0'}{1 - i(\tilde{\Delta}_\alpha + \tilde{x})}. \quad (B6)$$

Differentiating Eq. (B4) using $\tilde{\Delta}'_\alpha = \tilde{s}$ and $\tilde{x}' = \tilde{p}_x$ gives

$$\tilde{\alpha}'_0 = \frac{i(\tilde{s} + \tilde{p}_x)}{[1 - i(\tilde{\Delta}_\alpha + \tilde{x})]^2}. \tag{B7}$$

Substituting this into Eq. (B6) then gives us $\tilde{\alpha}_1$, which we can use to compute $|\tilde{\alpha}|^2$ to first order in $\tilde{\varepsilon}$:

$$|\tilde{\alpha}^2| = \frac{1}{1 + (\tilde{x} + \tilde{\Delta}_\alpha)^2} + \tilde{\varepsilon}\frac{4(\tilde{p}_x + \tilde{s})(\tilde{x} + \tilde{\Delta}_\alpha)}{[1 + (\tilde{x} + \tilde{\Delta}_\alpha)^2]^3} + \mathcal{O}(\tilde{\varepsilon}^2). \tag{B8}$$

The equations of motion to first order in $\tilde{\varepsilon}$ are then

$$\tilde{x}' = \tilde{p}_x,$$

$$\tilde{p}'_x = -\tilde{g} + \frac{1}{1 + (\tilde{x} + \tilde{\Delta}_\alpha)^2} + \tilde{\varepsilon}\frac{4(\tilde{p}_x + \tilde{s})(\tilde{x} + \tilde{\Delta}_\alpha)}{[1 + (\tilde{x} + \tilde{\Delta}_\alpha)^2]^3}. \tag{B9}$$

APPENDIX C: THE ADIABATIC APPROXIMATION

Here we provide more detail on the results from the adiabatic approximation in Sec. II B. We begin with the equations of motion Eq. (10)

$$\tilde{x}' = \tilde{p}_x,$$

$$\tilde{p}'_x = -\tilde{g} + \frac{1}{1 + (\tilde{\Delta}_\alpha + \tilde{x})^2}. \tag{C1}$$

Partially integrating the equation of motion for $\tilde{p}'_x$ with respect to $\tilde{x}$ gives

$$-\int\left(\frac{d\tilde{p}_x}{d\tilde{\tau}}\right)d\tilde{x} = \tilde{g}\tilde{x} - \arctan(\tilde{\Delta}_\alpha + \tilde{x}). \tag{C2}$$

As the dynamics are unchanged by a constant shift in the potential, we define the effective dimensionless potential energy as

$$\tilde{V}(\tilde{x}) = \tilde{g}(\tilde{\Delta}_\alpha + \tilde{x}) - \arctan(\tilde{\Delta}_\alpha + \tilde{x}). \tag{C3}$$

Then we can verify that $\tilde{p}'_x = -\nabla\tilde{V}(\tilde{x})$. Adding a "kinetic energy" term $(\tilde{p}'_x)^2/2$, the total dimensionless energy is defined as

$$\tilde{\mathcal{E}}(\tilde{x}, \tilde{p}_x) = \frac{\tilde{p}_x^2}{2} + \tilde{V}(\tilde{x}). \tag{C4}$$

We can verify that $\tilde{\mathcal{E}}$ is conserved by directly computing

$$\frac{d\tilde{\mathcal{E}}}{d\tilde{\tau}} = \tilde{p}_x\frac{d\tilde{p}_x}{d\tilde{\tau}} + \frac{d\tilde{V}}{d\tilde{x}}\frac{d\tilde{x}}{d\tilde{\tau}},$$

$$= \tilde{p}_x\left(-\frac{d\tilde{V}(\tilde{x})}{d\tilde{x}}\right) + \frac{d\tilde{V}}{d\tilde{x}}(\tilde{p}_x), \tag{C5}$$

$$= 0.$$

Thus in the adiabatic limit, the levitated mirror will behave like a classical particle moving in the potential Eq. (C3).

To find the frequency of these oscillations we follow the procedure outlined in Ref. [39, Sec. 2]. Suppose the mirror oscillates between two points $\tilde{x}_M$ and $\tilde{x}_P$. We necessarily have $\tilde{V}(\tilde{x}_M) = \tilde{V}(\tilde{x}_P)$, and $-\tilde{\sigma} < \tilde{x}_M < \tilde{\sigma} < \tilde{x}_P$. The dimensionless period $\tilde{\mathcal{T}}$ of an oscillation is

$$\tilde{\mathcal{T}} = \oint d\tilde{\tau} = 2\int_{\tilde{x}_M}^{\tilde{x}_P}\left(\frac{d\tilde{\tau}}{d\tilde{x}}\right)d\tilde{x}, \tag{C6}$$

which can be redimensionalized as $\mathcal{T} = \tilde{\mathcal{T}}/\nu$. We have $\frac{d\tilde{\tau}}{d\tilde{x}} = (\frac{d\tilde{x}}{d\tilde{\tau}})^{-1} = (\tilde{p}_x)^{-1}$, and we can write this in terms of the dimensionless energy using Eq. (12):

$$\tilde{\mathcal{T}} = \sqrt{2}\int_{\tilde{x}_M}^{\tilde{x}_P}\frac{d\tilde{x}}{\sqrt{\tilde{\mathcal{E}}(\tilde{x}, \tilde{p}_x) - \tilde{V}(\tilde{x})}}. \tag{C7}$$

Since energy is conserved in the adiabatic regime, over the whole period we have

$$\tilde{\mathcal{E}}(\tilde{x}, \tilde{p}_x) = \tilde{V}(\tilde{x}_M), \tag{C8}$$

and so the integral in Eq. (C7) can be evaluated. To find all periods, we choose $\tilde{x}_M \in (-\tilde{\sigma}, \tilde{\sigma})$, and then numerically solve the transcendental equation $\tilde{V}(\tilde{x}) = \tilde{V}(\tilde{x}_M)$ whose solution is $\tilde{x}_P$ (choosing the root which lies to the right of $\tilde{\sigma}$). Once $\tilde{x}_M$ and $\tilde{x}_P$ are in hand we may numerically compute the integral in Eq. (C7). The range of possible amplitudes increases as $\tilde{g}$ decreases since the width of the potential well increases. We plot the frequencies in Fig. 2(c) (rather than the period since $\tilde{\mathcal{T}}$ approaches infinity for the maximum amplitude oscillations). Note that the frequency of oscillation depends solely on the dimensionless parameter $\tilde{g}$ and the amplitude of oscillation, and furthermore the frequency decreases as the amplitude increases.

So far we assumed that the input laser detuning $\tilde{\Delta}_\alpha$ is static. We will now briefly investigate allowing $\tilde{\Delta}_\alpha$ to vary linearly with $\tilde{\tau}$, which can occur when we scan the cavity length or laser frequency

$$\tilde{\Delta}_\alpha(\tilde{\tau}) = \tilde{\Delta}_{\alpha0} + \tilde{s}\tilde{\tau}, \tag{C9}$$

where $\tilde{\Delta}_{\alpha0}$ is the initial detuning and $\tilde{s}$ the scan speed. Such a sweeping is commonly used to probe and characterize the optical system, and will correspond to shifting the potential shown in Fig. 2(a) horizontally at the speed $\tilde{s}$.

First suppose that $\tilde{\Delta}_{\alpha0}$ is negative (i.e., the laser is red-detuned compared to the cavity), and $\tilde{s}$ is positive. The mirror begins at $\tilde{x} = 0$, and we assume this to be sitting on a stand which prevents it from falling below this point. The potential $\tilde{V}$ is initially centered at $-\tilde{\Delta}_{\alpha0} > 0$, and moves to the left at speed $\tilde{s}$. The force due to the potential on the mirror is initially downwards, so the mirror will be stationary due to the stand. When $\tilde{\Delta}_\alpha(\tilde{\tau}) = -\tilde{\sigma}$ the local maximum of the potential will pass the mirror leading to a net upwards force, and so it will begin to oscillate on the stand. Eventually, however, the potential will keep moving and the force on the mirror will become negative; the oscillations will cease and it will rest on the stand.

The other case is for $\tilde{\Delta}_{\alpha0} > 0$ and $\tilde{s} < 0$, where the center of the potential begins to the left of the mirror and moves towards the right. If the scan speed is slow enough, the mirror will be "picked up" by the potential well and there will be oscillations centered about $\tilde{x} = \tilde{\Delta}_\alpha(\tilde{\tau})$. If the scan is too fast, however, the moving potential well will not be able to pick up the mirror, so after a brief period of oscillation the force will become downwards again and oscillations will cease. The critical scan velocity $\tilde{s}_c$ below which the mirror is picked up can be found by moving to a reference frame where the potential is stationary, while the mirror moves to the left at speed $\tilde{s}$. Because of the stand, the mirror does not begin moving until the force is in the upwards direction, and so

the initial mirror position in this frame must be at the local minimum of the potential well. In this case for the mirror to be trapped by the potential we require its kinetic energy to be less than the potential barrier between $\tilde{\sigma}$ and $-\tilde{\sigma}$:

$$\frac{\tilde{s}^2}{2} \leqslant 2[\arctan(\tilde{\sigma}) - \tilde{\sigma}\,\tilde{g}], \tag{C10}$$

which gives

$$\tilde{s}_c = 2\sqrt{\arctan(\tilde{\sigma}) - \tilde{\sigma}\,\tilde{g}}. \tag{C11}$$

APPENDIX D: CALCULATION OF THE PHOTOTHERMAL DISSIPATION RATE

Here we will investigate whether photothermal effects lead to damping or antidamping. To focus on the photothermal effect alone, we eliminate the influence of the optical field by making an adiabatic approximation. This is justified as typically the dynamics of the light field, described by $\tilde{\varepsilon}^{-1}$, are fast compared to the photothermal relaxation rate $\tilde{\gamma}$. With this we have equations of motion

$$\tilde{x}' = \tilde{p}_x,$$
$$\tilde{p}'_x = -\tilde{g} + \frac{1}{1 + (\tilde{\Delta}_\alpha + \tilde{x} + \tilde{z})^2},\tag{D1}$$
$$\tilde{z}' = -\tilde{\gamma}\left[\tilde{z} + \tilde{\xi}\frac{1}{1 + (\tilde{\Delta}_\alpha + \tilde{x} + \tilde{z})^2}\right].$$

We then linearize the system Eq. (D1) about the steady state $\tilde{x}^s_+$, leading to equations of motion

$$\delta\tilde{x}' = \delta\tilde{p}_x,$$
$$\delta\tilde{p}'_x = -\tilde{\omega}^2(\delta\tilde{x} + \delta\tilde{z}),\tag{D2}$$
$$\delta\tilde{z}' = \tilde{\gamma}\tilde{\xi}\tilde{\omega}^2\delta\tilde{x} - \tilde{\lambda}\delta\tilde{z},$$

with constants defined as

$$\tilde{\omega}^2 = 2\tilde{g}^2\sqrt{\frac{1}{\tilde{g}} - 1}, \quad \tilde{\lambda} = \tilde{\gamma}(1 - \tilde{\omega}^2\tilde{\xi}).\tag{D3}$$

While the coupled linear system Eq. (D2) can be solved directly, this results in a very complicated expression. We can, however, derive a simpler approximate solution, taking advantage of the small value of $\tilde{\gamma}$.

Suppose that the mirror is perturbed slightly from $\tilde{x}^s_+$. From our analysis of the adiabatic system in Sec. II B we know that the mirror will oscillate around the steady state. As this happens, this will induce oscillations in the intracavity field, and thus photothermal expansion $\delta\tilde{z}$. Due to the small value of $\tilde{\gamma}$, the oscillations of $\delta\tilde{z}$ will be much smaller than those of $\delta\tilde{x}$ and $\delta\tilde{p}_x$. A zeroth-order approximation will thus be to take $\delta\tilde{z} \approx \mathcal{O}(\tilde{\gamma}) \approx 0$, in which case we find from Eq. (D2)

$$\delta\tilde{x}(\tilde{\tau}) = \tilde{\rho}\sin(\tilde{\omega}\tilde{\tau}),$$
$$\delta\tilde{p}_x(\tilde{\tau}) = \tilde{\rho}\tilde{\omega}\cos(\tilde{\omega}\tilde{\tau}),\tag{D4}$$
$$\delta\tilde{z}(\tilde{\tau}) = 0,$$

where $\tilde{\rho}$ is the size of the perturbation to $\delta\tilde{x}$. We can then substitute Eq. (D4) into the equations of motion Eq. (D2) to calculate the error, which we find to be $\mathcal{O}(\tilde{\gamma})$.

Next we use Eq. (D4) to generate the first-order approximation. We assume $\delta\tilde{x}, \delta\tilde{p}_x$ take the form given in Eq. (D4), and then solve the equation of motion for $\delta\tilde{z}'$ which yields

$$\delta\tilde{z}(\tilde{\tau}) = \frac{\tilde{\rho}\tilde{\omega}^2\tilde{\gamma}\tilde{\xi}}{\tilde{\omega}^2 + \tilde{\lambda}^2}(\tilde{\lambda}\sin(\tilde{\omega}\tilde{\tau}) - \tilde{\omega}\cos(\tilde{\omega}\tilde{\tau})). \tag{D5}$$

We then substitute in this form for $\delta\tilde{z}$ into the equations of motion Eq. (D2), and derive

$$\delta\tilde{x}(\tilde{\tau}) = \tilde{\rho}\sin(\tilde{\omega}\tilde{\tau}) + \tilde{\rho}\tilde{\gamma}\tilde{E}(\tilde{C}_+(\tilde{\tau})\cos(\tilde{\omega}\tilde{\tau})$$
$$- \tilde{D}_-(\tilde{\tau})\sin(\tilde{\omega}\tilde{\tau})),$$
$$\delta\tilde{p}_x(\tilde{\tau}) = \tilde{\rho}\omega\cos(\tilde{\omega}\tilde{\tau}) + \tilde{\rho}\tilde{\gamma}\tilde{\omega}\tilde{E}(\tilde{D}_+(\tilde{\tau})\cos(\tilde{\omega}\tilde{\tau})$$
$$+ \tilde{C}_-(\tilde{\tau})\sin(\tilde{\omega}\tilde{\tau})),\tag{D6}$$

where

$$\tilde{E} = \frac{\tilde{\xi}\tilde{\omega}^2}{4(\tilde{\omega}^2 + \tilde{\lambda}^2)},$$
$$\tilde{C}_\pm(\tilde{\tau}) = \tilde{\omega}(1 \pm 2\tilde{\lambda}\tilde{\tau}),\tag{D7}$$
$$\tilde{D}_\pm(\tilde{\tau}) = \tilde{\lambda} \pm 2\tilde{\omega}^2\tilde{\tau}.$$

Substituting Eqs. (D5) and (D6) into the equations of motion Eq. (D2) the error is found to be of order $\mathcal{O}(\tilde{\gamma}^2\tilde{\tau})$, which is negligible for small times. We can thus use these approximate solutions to see how the photothermal expansion will affect the stability of $\tilde{x}^s_+$.

Accounting for photothermal expansion, the energy of the mirror is now

$$\tilde{\mathcal{E}} = \frac{\tilde{p}_x^2}{2} + \tilde{g}\tilde{x} - \tan^{-1}(\tilde{x} + \tilde{z}). \tag{D8}$$

Assuming we are in the neighbourhood of the steady state $(\tilde{x}^s_+, \tilde{p}^s_x, \tilde{z}^s)$, we have to second order

$$\tilde{\mathcal{E}} = \tilde{\mathcal{E}}^s - \tilde{g}\delta\tilde{z} + \frac{\delta\tilde{p}_x^2}{2} + \frac{\tilde{\omega}^2}{2}(\delta\tilde{x} + \delta\tilde{z})^2 + \mathcal{O}(\delta^3), \tag{D9}$$

where $\tilde{\mathcal{E}}^s$ is the steady-state energy. If the mirror position is perturbed a distance $\tilde{\rho}$ from equilibrium, its motion will approximate periodic oscillation with period

$$\tilde{T} = \frac{2\pi}{\tilde{\omega}}. \tag{D10}$$

The average heating over a single oscillation can then be found via

$$\frac{1}{\tilde{T}}\int_0^{\tilde{T}}\frac{d\tilde{\mathcal{E}}}{d\tilde{\tau}}d\tilde{\tau}. \tag{D11}$$

Using the derived forms Eqs. (D5) and (D6), we find this to be

$$\frac{\tilde{\omega}^4}{2}\tilde{\rho}^2\tilde{\xi}\tilde{\gamma} + \mathcal{O}(\tilde{\gamma}^2) = 2(1 - \tilde{g})\tilde{g}^3\tilde{\rho}^2\tilde{\xi}\tilde{\gamma} + \mathcal{O}(\tilde{\gamma}^2). \tag{D12}$$

Thus photothermal expansion induces antidamping at a rate linearly proportional to $\tilde{\xi}$: positive photothermal expansion will provide an antidamping effect, while negative photothermal expansion will give damping.

[1] M. Aspelmeyer, T. J. Kippenberg, and F. Marquard, Rev. Mod. Phys. **86**, 1391 (2014).

[2] A. Pontin, M. Bonaldi, A. Borrielli, F. Cataliotti, F. Marino, G. Prodi, E. Serra, and F. Marin, Phys. Rev. A **89**, 023848 (2014).

[3] S. Gröblacher, J. B. Hertzberg, M. R. Vanner, G. D. Cole, S. Gigan, K. Schwab, and M. Aspelmeyer, Nat. Phys. **5**, 485 (2009).

[4] S. Mancini, V. Man'ko, and P. Tombesi, Phys. Rev. A **55**, 3042 (1997).

[5] V. Fiore, Y. Yang, M. C. Kuzyk, R. Barbour, L. Tian, and H. Wang, Phys. Rev. Lett. **107**, 133601 (2011).

[6] S. Bose, K. Jacobs, and P. L. Knight, Phys. Rev. A **59**, 3204 (1999).

[7] H. Yang, H. Miao, D.-S. Lee, B. Helou, and Y. Chen, Phys. Rev. Lett. **110**, 170401 (2013).

[8] C. C. Gan, C. M. Savage, and S. Z. Scully, Phys. Rev. D **93**, 124049 (2016).

[9] A. Großardt, J. Bateman, H. Ulbricht, and A. Bassi, Phys. Rev. D **93**, 096003 (2016).

[10] F. Marino, F. S. Cataliotti, A. Farsi, M. S. de Cumis, and F. Marin, Phys. Rev. Lett. **104**, 073601 (2010).

[11] A. H. Safavi-Naeini, S. Gröblacher, J. T. Hill, J. Chan, M. Aspelmeyer, and O. Painter, Nature **500**, 185 (2013).

[12] Z. Hao, A. Erbil, and F. Ayazi, Sens. Actuators, A **109**, 156 (2003).

[13] R. A. Norte, J. P. Moura, and S. Gröblacher, Phys. Rev. Lett. **116**, 147202 (2016).

[14] Y. Tsaturyan, A. Barg, E. S. Polzik, and A. Schliesser, Nat. Nanotechnol. **12**, 776 (2017).

[15] M. Bhattacharya, A. N. Vamivakas, and P. Barker, J. Opt. Soc. Am. B **34**, LO1 (2017).

[16] K. G. Libbrecht and E. D. Black, Phys. Lett. A **321**, 99 (2004).

[17] A. Arvanitaki and A. A. Geraci, Phys. Rev. Lett. **110**, 071105 (2013).

[18] N. Kiesel, F. Blaser, U. Delić, D. Grass, R. Kaltenbaek, and M. Aspelmeyer, Proc. Natl. Acad. Sci. USA **110**, 14180 (2013).

[19] O. Romero-Isart, A. C. Pflanzer, M. L. Juan, R. Quidant, N. Kiesel, M. Aspelmeyer, and J. I. Cirac, Phys. Rev. A **83**, 013803 (2011).

[20] S. Singh, G. Phelps, D. Goldbaum, E. M. Wright, and P. Meystre, Phys. Rev. Lett. **105**, 213602 (2010).

[21] T. Corbitt, Y. Chen, E. Innerhofer, H. Müller-Ebhardt, D. Ottaway, H. Rehbein, D. Sigg, S. Whitcomb, C. Wipf, and N. Mavalvala, Phys. Rev. Lett. **98**, 150802 (2007).

[22] K.-K. Ni, R. Norte, D. Wilson, J. Hood, D. Chang, O. Painter, and H. Kimble, Phys. Rev. Lett. **108**, 214302 (2012).

[23] D. Chang, K. Ni, O. Painter, and H. Kimble, New J. Phys. **14**, 045002 (2012).

[24] H. J. Slatyer, G. Guccione, Y. W. Cho, B. C. Buchler, and P. K. Lam, J. Phys. B: At., Mol. Opt. Phys. **49**, 125401 (2016).

[25] G. Guccione, M. Hosseini, S. Adlong, M. T. Johnsson, J. Hope, B. C. Buchler, and P. K. Lam, Phys. Rev. Lett. **111**, 183001 (2013).

[26] Y. Michimura, Y. Kuwahara, T. Ushiba, N. Matsumoto, and M. Ando, Opt. Express **25**, 13799 (2017).

[27] C. Ho, R. B. Mann, and T. C. Ralph, arXiv:1911.02705.

[28] A. Ashkin, Phys. Rev. Lett. **24**, 156 (1970).

[29] I. Verdeny, A. Farré, J. Mas Soler, C. López Quesada, E. Martín Badosa, and M. Montes Usategui, Óptica Pura y Aplicada **44**, 527 (2011).

[30] R. Lecamwasam, To download code for this manuscript, visit github.com/ruvilecamwasam/lmdynamics, (2019).

[31] F. Marino, M. De Rosa, and F. Marin, Phys. Rev. E **73**, 026217 (2006).

[32] F. Marino and F. Marin, Phys. Lett. A **364**, 441 (2007).

[33] F. Marino and F. Marin, Phys. Rev. E **83**, 015202(R) (2011).

[34] F. Marino and F. Marin, Phys. Rev. E **87**, 052906 (2013).

[35] M. De Rosa, L. Conti, M. Cerdonio, M. Pinard, and F. Marin, Phys. Rev. Lett. **89**, 237402 (2002).

[36] K. Konthasinghe, J. G. Velez, A. J. Hopkins, M. Peiris, L. T. Profeta, Y. Nieves, and A. Muller, Phys. Rev. A **95**, 013826 (2017).

[37] D. Kelley, J. Lough, F. Mangaña-Sandoval, A. Perreca, and S. W. Ballmer, Phys. Rev. D **92**, 062003 (2015).

[38] N. G. Van Kampen, Phys. Rep. **124**, 69 (1985).

[39] P. Amore and F. M. Fernández, Eur. J. Phys. **26**, 589.